The AAPS Journal, Vol. 14, No. 4, December 2012 (© 2012)
DOI: 10.1208/s12248-012-9379-9

Research Article

Effect of Device Design on the *In Vitro* Performance and Comparability for Capsule-Based Dry Powder Inhalers

Jagdeep Shur,[1] Sau Lee,[2,3] Wallace Adams,[2] Robert Lionberger,[2] James Tibbatts,[1] and Robert Price[1]

Received 26 March 2012; accepted 24 May 2012; published online 22 June 2012

Abstract. This study investigated the effect of modifying the design of the Cyclohaler on its aerosolization performance and comparability to the HandiHaler at multiple flow rates. The Cyclohaler and HandiHaler were designated as model test and reference unit-dose, capsule-based dry powder inhalers (DPIs), respectively. The flow field, pressure drop, and carrier particle trajectories within the Cyclohaler and HandiHaler were modeled via computational fluid dynamics (CFD). With the goal of achieving *in vitro* comparability to the HandiHaler, the CFD results were used to identify key device attributes and to design two modifications of the Cyclohaler (Mod 1 and Mod 2), which matched the specific resistance of the HandiHaler but exhibited different cyclonic flow conditions in the device. Aerosolization performance of the four DPI devices was evaluated by using the reference product's capsule and formulation (Spiriva capsule) and a multistage cascade impactor. The *in vitro* data showed that Mod 2 provided a closer match to the HandiHaler than the Cyclohaler and Mod 1 at 20, 39, and 55 l/min. The *in vitro* and CFD results together suggest that matching the resistance of test and reference DPI devices is not sufficient to attain comparable aerosolization performance, and the improved *in vitro* comparability of Mod 2 to the HandiHaler may be related to the greater degree of similarities of the flow rate of air through the pierced capsule (Q_c) and the maximum impact velocity of representative carrier particles (V_n) in the Cyclohaler-based device. This investigation illustrates the importance of enhanced product understanding, in this case through the CFD modeling and *in vitro* characterization of aerosolization performance, to enable identification and modification of key design features of a test DPI device for achieving comparable aerosolization performance to the reference DPI device.

KEY WORDS: computational fluid dynamics; device design; dry powder inhaler; *in vitro* comparability; *in vitro* performance.

INTRODUCTION

The use of dry powder inhalers (DPIs) for treatment of asthma and chronic obstructive pulmonary disease has become increasingly common in the USA (1). With a number of patent expirations of innovator DPI products looming, a major challenge for generic DPI entry is understanding design factors that can alter the product performance of the generic DPI such that it can demonstrate bioequivalence (BE) to the innovator product (2).

As locally acting DPIs do not rely on the systemic circulation for targeting the site(s) of action, the approach for establishing BE of these orally inhaled drug products in the USA is based on the aggregate weight of scientific evidence that includes device and formulation comparability, equivalence in a number of *in vitro* tests, and *in vivo* equivalence in local drug delivery and systemic exposure (3). It has been reported that there is inter- and intrasubject variability in patient's peak inhalation flow through DPIs, which is in part linked to the severity of airway disease (4). Thus, it is important for the *in vitro* performance of a test DPI to match that of the reference DPI across different flow rates.

The local delivery of drug(s) to the lung from a passive DPI depends on a combination of device and formulation properties along with the inspiratory flow of the patient (5). The complex relationship between the physicochemical properties of the powder dose and the design of the DPI device will ultimately control the fluidization, deaggregation, and aerodynamic particle size of the drug particles (6). This in turn will influence the regional deposition of drug particles in the lung and thus the safety and efficacy of a DPI (7). Hence, in order to produce a test DPI that closely matches the *in vitro* performance of the reference DPI, it is important to investigate the fluidization and deaggregation behavior of the

The opinions expressed in this paper by the authors do not necessarily reflect the views or policies of the Food and Drug Administration (FDA).

Electronic supplementary material The online version of this article (doi:10.1208/s12248-012-9379-9) contains supplementary material, which is available to authorized users.

[1] Pharmaceutical Surface Science Research Group, Department of Pharmacy and Pharmacology, University of Bath, Claverton Down, Bath, BA2 7AY, UK.
[2] Office of Generic Drugs, Center for Drug Evaluation and Research, US Food and Drug Administration, 7519 Standish Place, Rockville, Maryland 20855, USA.
[3] To whom correspondence should be addressed. (e-mail: sau.lee@fda.hhs.gov)

dose in both test and reference DPI devices. For such investigations, it is critical to identify the key design features of both test and reference DPI devices and understand their effect on the aerosolization performance.

It is generally believed that significant differences in the specific resistance of test and reference DPIs may lead to significant differences in drug delivery performance (6,8). The internal "force" required for fluidization and deaggregation is dependent on the resistance of the DPI device and the patient's inspiratory effort (9). Thus, for the purpose of increasing the likelihood of establishing comparable *in vitro* performance and *in vivo* drug deposition, the specific resistance of a test device should be comparable to the reference device. Furthermore, variations in the fluid dynamics of an entrained airflow of DPIs may influence powder dispersion (10). This highlights the significance of modeling and understanding the complex nature of the flow field in the test and reference devices. Hence, when considering the development of a test DPI, it is important to consider modifications that will produce a test device that not only has comparable pressure drops across a range of flow rates, but in which the aerosolization performance of the test DPI device has been manipulated to match that of the reference DPI device.

Computational fluid dynamics (CFD) is an established methodology for predicting the flow properties and the fate of the particulate system in the respiratory tract and inhalation devices (10–20). For example, Coates *et al.* demonstrated how CFD modeling of the DPI mouthpiece geometry, dispersion grid and air inlet size (11), airflow rate (12), and capsule properties (13) could be used to investigate aerosol performance. In addition, the recent work by Donovan *et al.* utilized CFD to investigate the aerosolization performance of carrier particles of different physical properties in the Aerolizer and HandiHaler. They found that in comparison to the HandiHaler, the aerosolization performance of the Aerolizer was more dependent on the carrier particle size, which appeared to be related to a greater number of carrier particle–inhaler collisions (17). Despite these studies, there are no examples that utilize CFD modeling to define device design parameters, in order to achieve *in vitro* comparability of two different unit-dose, capsule-based DPI devices of different designs across multiple flow rates.

The aim of this study was to identify the key device attributes and evaluate the effect of their modifications on the aerosolization performance for unit-dose, capsule-based DPI devices, by utilizing CFD modeling and *in vitro* characterization by a multistage cascade impactor (CI). Specifically, this study was designed to assess whether two different test and reference DPI devices, after appropriate modification(s) of the test DPI device, could deliver comparable aerosolization performance at three flow rates. The DPI devices investigated included the Spiriva HandiHaler, Cyclohaler (similar to the Aerolizer in the USA), and two modified Cyclohalers that were manufactured as part of the study. The HandiHaler was selected as a model reference DPI device. The Cyclohaler was utilized as a model test device to represent an alternative DPI. The HandiHaler and Cyclohaler differ in terms of both the device resistance and airflow behavior. The specific resistance of the Cyclohaler ($0.018\ kPa^{0.5}/(l\ min^{-1})$) is considerably lower than that of the HandiHaler ($0.049\ kPa^{0.5}/(l\ min^{-1})$) (17,21). The development of the two additional test DPI devices (referred to as Mod 1 and Mod 2) was based on the Cyclohaler platform with knowledge gained from the CFD simulations of the Cyclohaler, as explained below. In order to isolate the influence of the device from that of the formulation and capsule on the aerosolization performance, the reference product formulation (Spiriva capsule) was used in all cases for CI measurements. Based on the paper by Lee *et al.* (3), the flow rates of 20, 39, and 55 l/min were selected for CFD and CI comparisons of the test and reference DPI devices, given that the HandiHaler was selected as the reference DPI in this study. These three flow rates are expected to reasonably cover the inspiratory flow rates through the DPI, generated by relevant patient populations, as described in the labeling of Spiriva HandiHaler.

MATERIALS AND METHODS

Materials

The Spiriva HandiHaler drug product consists of capsules and a unit-dose, capsule-based DPI device. Each Spiriva capsule contains 18 μg tiotropium (equivalent to 22.5 μg tiotropium bromide monohydrate) blended with lactose monohydrate as the carrier. The powder formulation is contained in a size 3 hard gelatin capsule. The fill weight of the formulation is approximately 5 mg, which is presented in the capsule as a small agglomerated mass of powder.

Tiotropium bromide monohydrate, supplied by Sigma-Aldrich (Poole, UK), was used to prepare standards for analytical quantification by high performance liquid chromatography (HPLC). All solvents used were HPLC grade (Fisher Chemicals, Loughborough, UK). Ultrapure water was produced by reverse osmosis (MilliQ, Millipore, Molsheim, France). Commercial samples of the HandiHaler (batch number, 956681; expiry date, April 2011) and Cyclohaler were supplied by AAH Pharmaceuticals Ltd. (Coventry, UK). Note that the commercial samples of the HandiHaler were within the expiry at the time of testing. Both Mod 1 and Mod 2 were prepared by stereolithography using the same resin materials and were manufactured by Concept Flow Ltd. (Coton, UK). The materials of construction for HandiHaler, Cyclohaler, and the modified Cyclohalers may differ. However, the device material properties and their possible effect on the *in vitro* performance were not investigated as part of this study.

Particle Size Analysis by Laser Diffraction

Particle size distributions of all samples were measured in the wet state using a Sympatec HELOS and CUVETTE laser diffraction system (Sympatec GmbH, Clausthal-Zellerfeld, Germany) with an R4 lens (0.5–350 μm). Approximately 5 mg of powder was suspended in HPLC grade cyclohexane saturated with lactose monohydrate. The lactose-saturated cyclohexane also contained 0.5% lecithin (Acros Organics, Geel, Belgium), which was produced using sonication for 5 min at 25°C and immediately transferred into a 50-ml cuvette to produce an appropriate optical concentration (10–25%). Each measurement was performed in triplicate, and particle size analysis was performed using WINDOX 5.0 software (Sympatec GmbH, Clausthal-Zellerfeld, Germany).

Computational Fluid Dynamics

CFD analysis (ANSYS Fluent 6.3) was utilized to evaluate the flow field, pressure drop, and particle trajectories within the different DPI devices at flow rates of 20, 39, and 55 l/min. The geometries of the HandiHaler and Cyclohaler devices were constructed from detailed measurements taken from the marketed devices using a micrometer. Modifications were made to the Cyclohaler to produce Mod 1 and Mod 2, which differ from the Cyclohaler only in terms of the air inlet dimension and geometry. Each of the geometries included a representation of the air inlet(s), capsule chamber, mesh, and mouthpiece. A pierced capsule was also included in the simulations to allow modeling of the entraining airflow drawn through the capsule's pierced hole. The capsule position and orientation in each case were chosen to approximate the capsule position, where a significant portion of powder was released from the capsule within the capsule chamber, as observed from the high-speed imaging upon exposure to airflow (not shown). In the Cyclohaler, Mod 1, and Mod 2, the capsule was positioned at the outside of the capsule cavity with its long axis aligned with the tangential direction. In the Handihaler, the capsule was positioned 7° off axis at the mesh end of the chamber. In all cases, the capsules were modeled based on the assumption of being pierced with open holes of matching diameter to the piercing pins. The positions of the hole in the CFD models were based on the measurement taken from the actual pierced capsules.

A computational mesh was then applied to each of the geometries including both the internal and external volumes of the capsule. Since the computational mesh was applied to both the internal and external volumes of the capsule, the models were set up to account for the flux of air into and out of the capsule shell via the pierced holes. This approach was chosen in order to enable the calculation of the airflow rate through the pierced capsule.

Prismatic boundary layers were applied to the surfaces of the capsule and the walls of the capsule chamber with a first cell height of 75 μm. Prismatic cells were also used in the mesh region, inlet geometry, and mouthpiece section of the device. Unstructured tetrahedral cells were applied within the remainder of the capsule chamber and within the capsule itself. The tetrahedral cells were then converted to polyhedral cells to reduce the skewness of the overall cell count. The conversion to polyhedral did not affect the height of the prism layers; therefore, the near-wall resolution was unaffected by this conversion. In the Cyclohaler device, Mod 1, and Mod 2, the initial tetrahedral meshes comprised approximately 2.8 million computational cells, which were converted to meshes of approximately 600,000 polyhedral cells. In the Handihaler device, a 1.6 million cell-tetrahedral mesh was converted to a mesh of 400,000 polyhedral cells. For all of the computational meshes, the average $y+$ value, which is representative of the near-wall resolution, was approximately 10. A mesh dependence study was conducted, which showed that the predicted results were not influenced by further increase in the computational mesh resolution. The flow field generated in each device was then calculated by solving the Reynolds-averaged Navier Stokes equations together with the realizable k–ε turbulence model (22) with standard wall functions (23). A Second-Order Upwind scheme was used to discretize the pressure equations, and a Quadratic Upwind Interpolation for Convection Kinetics scheme was used to discretize the momentum and turbulence equations. Both of these schemes provide second-order accuracy. The numerical equations were converged to a steady-state solution.

Approximately 1,500 steady-state Lagrangian particle tracks for spherical particles were calculated using Fluent's Discrete Phase Model (24) for each simulation. A 50-μm particle size was selected for comparison of aerosolization performance between the test and reference DPI devices. This particle size was within the size range of lactose carriers used in the Spiriva formulation (D_{10}=2 μm, D_{50}=25 μm, and D_{90}=98 μm), as measured by laser diffraction. The influence of particle size was investigated in a sensitivity study, and it was shown that the qualitative conclusions drawn from the comparative analysis of test and reference DPI devices were independent of the chosen particle size in the range of 25–75 μm.

A sensitivity study was conducted into the number of particle streams and into the sensitivity to stochastic tracking. It was shown that 500 particle streams were sufficient to provide solution independence, which implied that analysis with any greater number of particle streams would not affect the solutions reported in the present study. In addition, it was shown that stochastic tracking did not influence the results. This was due to the relatively high inertia of the 50-μm particle size, which is not influenced by local turbulent fluctuations. Since the solution was not sensitive to turbulence–particle interactions, no near-wall turbulence corrections were used in the simulations (25,26). A further study was conducted to investigate the influence of the coefficient of restitution. The study showed that the results were sensitive to the choice of coefficient of restitution. However, this sensitivity was not found to affect the qualitative conclusions that were drawn from the comparative analysis of test and reference DPI devices. Throughout the reported data, the normal coefficient of restitution was chosen to be 0.65, and the tangential coefficient of restitution was chosen to be 0.9.

The particle trajectories were solved using the spherical nonlinear drag law by Morsi and Alexander (27) as implemented in ANSYS Fluent (24). This law reduces to a Stokesian drag law at low Reynolds numbers, but follows an empirically derived drag law with Reynolds numbers greater than 1. The typical particle Reynolds numbers in the simulations were of the order 100. In all cases, the particle acceleration was significantly greater than the gravitational acceleration, so the gravitational contribution was neglected throughout the simulations. The particles were introduced into the solution domain at rest on a plane inside the capsule and were entrained into the capsule chamber by the airflow through the pierced capsule. However, particle statistics were only gathered once the particles were outside the capsule, where the mass loading of powder was sufficiently low that both mass loading and interparticle collisions were neglected.

High-Speed Laser Imaging

The Oxford Lasers EnVision (Didcot, UK) imaging system was used to capture the fluidization process and flow behavior inside the device. The light source utilized was the Oxford Lasers FireFLY pulsed diode laser, which was operated at a wavelength of 808 nm. The light source was pulsed so that images captured are free from motion blur, providing high-

quality images for use in more advanced analysis techniques. The imaging system was operated at 2,000 images per second at a resolution of 512×512 pixels. In order to visualize the powder movement inside the capsule, transparent size 3 HPMC capsules (Qualicaps, Basingstoke, UK) filled with 10 mg of sieved lactose (SV003, DFE Pharma, Vehgel, Netherlands) were used.

Airflow Resistance

The pressure drop of all devices was tested using a Copley Dose Uniformity Sampling Apparatus (DUSA, Copley Scientific, Nottingham, UK), Copley critical flow controller TPK (Copley Scientific, Nottingham, UK), and vacuum pump (GE Motors, MI, USA). For this assembly, the DUSA with the mouthpiece adapter was connected to the TPK, a flow meter (DFM 2000, Copley Scientific, Nottingham, UK), and a vacuum source. The pressure measurement port on the DUSA was connected to the TPK to enable measurement of the device pressure drop at a defined flow rate. A capsule was inserted into the device, and the flow rate was adjusted to achieve the desired flow rate, which was confirmed by the flow meter. In this way, the pressure drop was determined from the digital readout of the TPK at flow rates ranging between 10 and 90 l/min.

Cascade Impactor Measurements

The drug content was detected and quantified using HPLC. The HPLC system consisted of a pump coupled to an autosampler and multi-wavelength UV detector (Agilent 1200, Wokingham, UK) set at 240 nm. The pump flow rate was set to 1.8 ml/min through a Hypersil BDS-C_{18} column (Fisher Scientific, Loughborough, UK; length of the column, 250 mm; internal diameter, 4.6 mm; and particle size of the packing material, 5 μm), which was placed in a column oven (Agilent, Wokingham, UK) set to 25°C. The mobile phase included 70% perchloric acid and 30% water/acetonitrile (60:40 *v*/*v*). The elution time for the drug peak was 3.7 min. All standards were prepared in 0.1 mM HCl. A linear regression analysis was used for the assessment of HPLC calibration. Quantification was carried out by an external standard method, and linearity was verified between 0.05 and 50 μg/ml. The drug substance remained stable within the mobile phase system, and no drug degradation was observed during the measurements.

The *in vitro* aerosolization performances of the reference and test devices were performed using Spiriva capsules. Testing was performed using a Next Generation Impactor (NGI) with a pre-separator, which was connected to a vacuum pump (GE Motors, MI, USA). Prior to testing, the pre-separator was filled with 15 ml of 0.1 mM HCl as washing media. The NGI cups were coated with 1% *v*/*v* silicone oil in hexane to eliminate particle bounce. For each experiment, ten individual Spiriva capsules were discharged into the NGI using the reference or test devices at 20, 39, and 55 l/min for a duration of time representative of an inhaled volume of 4 l. Following aerosolization, the NGI apparatus was dismantled, and the inhaler, capsules, and each part of the NGI were washed down with 0.1 mM HCl into known volumes with the HPLC mobile phase. The mass of drug deposited on each stage and accessory, including the device and the capsule, of the NGI experiment was determined by HPLC. This protocol was repeated in triplicate for the HandiHaler, Cyclohaler, Mod 1, and Mod 2.

The emitted dose (ED), impactor-sized mass (ISM), mass median aerodynamic diameter (MMAD), and geometric standard deviation (GSD) were determined from the analysis of the NGI data. The ED was defined as the mass collected from the inlet port, pre-separator, and stages 1–8, and the ISM was defined by the mass of drug collected on stages 2–8 of the NGI. MMAD and GSD were calculated based upon the inverse normals of the cumulative percentage under the stated aerodynamic diameter *versus* the log of the effective cutoff diameter. Linear regression of the five data points closest to 50% of the cumulative particle mass that entered the CI was performed to compute the MMAD and GSD. The cutoff diameters were calculated and corrected for the different flow rates utilized in the study according to USP <601> (28). In all CI tests conducted, the mass balance was within ±15% of the total recovered dose.

RESULTS

CFD Modeling of the HandiHaler

The CFD model of the HandiHaler shows that the device consists of a capsule chamber with its bottom connected to the chamber inlet, which is a primary flow inlet (Fig. 1a). The capsule is inserted in the vertical position, and rests over the chamber inlet. Above the capsule chamber is a metallic convex mesh, which sits over the by-pass inlets and the capsule. Donovan *et al.* have reported a similar CFD model of the HandiHaler (17).

The pressure and velocity distributions within the capsule chamber of the HandiHaler, as well as the pressure distribution on the whole capsule, are shown in Fig. 2. The pressure distribution within the HandiHaler (Fig. 2a) indicates that all of the pressure loss within this device occurs across the orifice at the beginning of that inlet. While the CFD simulations shown are calculated for 39 l/min, these data are representative of the static pressures acting in the device and capsule and air velocity magnitude at 20 and 55 l/min. These data suggest that the dimensions of this orifice primarily determine the resistance of the HandiHaler, which has also been suggested by Donovan *et al.* (17).

The velocity distribution profile within the capsule chamber of the HandiHaler indicates that the inlet orifice generates a high-velocity air jet at the base of the capsule (Fig. 2b). This corresponds with the generation of a pressure gradient at the hemispherical base of the capsule (Fig. 2c). Consistent with the observation by Wachtel *et al.* and

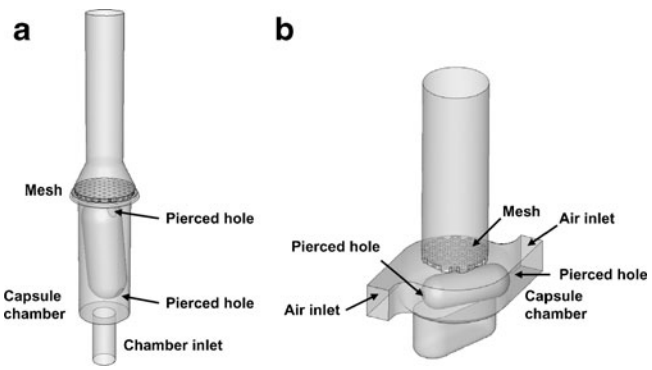

Fig. 1. Schematic illustrations of the **a** HandiHaler and **b** Cyclohaler

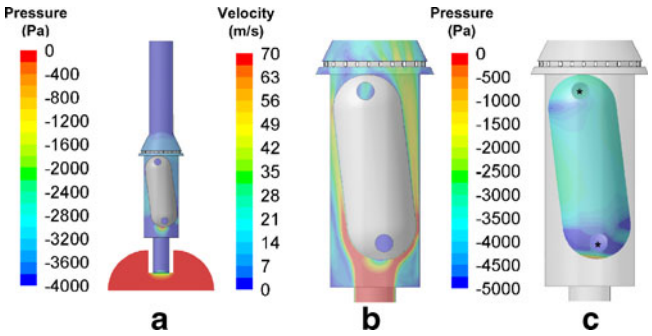

Fig. 2. CFD predictions of **a** the pressure and **b** velocity profiles within the HandiHaler, as well as **c** the pressure profile of the whole capsule within the HandiHaler at 39 l/min. The *circles* indicate the pierced holes in the capsules

Donovan *et al.* (17,29), the incoming air pushes the capsule toward the mesh. However, as the airflow accelerates radially around the hemisphere, high air velocities close to the capsule wall result in an annular region of very low pressure, which pulls the capsule back toward the inlet end of the capsule chamber. At the inlet end of the chamber, the capsule experiences a net positive force, i.e., the capsule is accelerated back toward the mesh end of the chamber. This behavior would suggest that the capsule is likely to vibrate axially within the capsule chamber. The sequential high-speed video images (Fig. 1 in Supplementary Materials) depict the axial vibration of the capsule within the capsule chamber. This axial movement of the capsule persists throughout the operation of the device. In addition to the vibration of the capsule, the pressure distribution calculated by CFD around the capsule also indicates that the airflow is driven through the pierced hole in the capsule. Specifically, as the lower pierced hole is situated within the annular low-pressure region, the air is drawn into the capsule through the upper pierced hole and then out from the lower pierced hole. This helps to entrain the powder dose and causes the majority of the powder dose to leave the capsule through the lower pierced hole. This is consistent with the high-speed imaging data (not shown).

CFD Modeling of the Cyclohaler and Modified Cyclohaler Devices

The Cyclohaler consists of a mouthpiece that has a mesh enclosing the capsule chamber, as illustrated by the CFD model in Fig. 1b. In addition, Fig. 3 shows the pressure and velocity distributions in the device as well as the pressure distribution on the capsule at 39 l/min airflow. These data are also representative of the pressure and velocity distributions in the device and capsule at 20 and 55 l/min. The capsule chamber has a capsule enclosure area and two tangential air inlets at diagonally opposite positions of the capsule chamber. The mesh sits on the top of the capsule chamber and retains the capsule within the chamber during inhalation. The flow structure within the Cyclohaler is predominantly swirling or cyclonic flow. The tangential inlets to the capsule chamber introduce air to the capsule chamber with significant tangential momentum (Fig. 3b). In order for the air to exit through the mesh, a radial pressure gradient is set up within the capsule chamber (Fig. 3a). The pressure distribution within the Cyclohaler indicates that the resistance of the device is dependent on the dimension of tangential air inlets, from which about 50% of the pressure is lost. The remainder of the pressure loss is due to the mesh (data not shown), which is consistent with the findings of Coates *et al.* (11). In addition, Fig. 3b suggests that the airflow is accelerated through the tangential inlets and sets up a cyclonic flow within the capsule chamber. Hence, changes to the

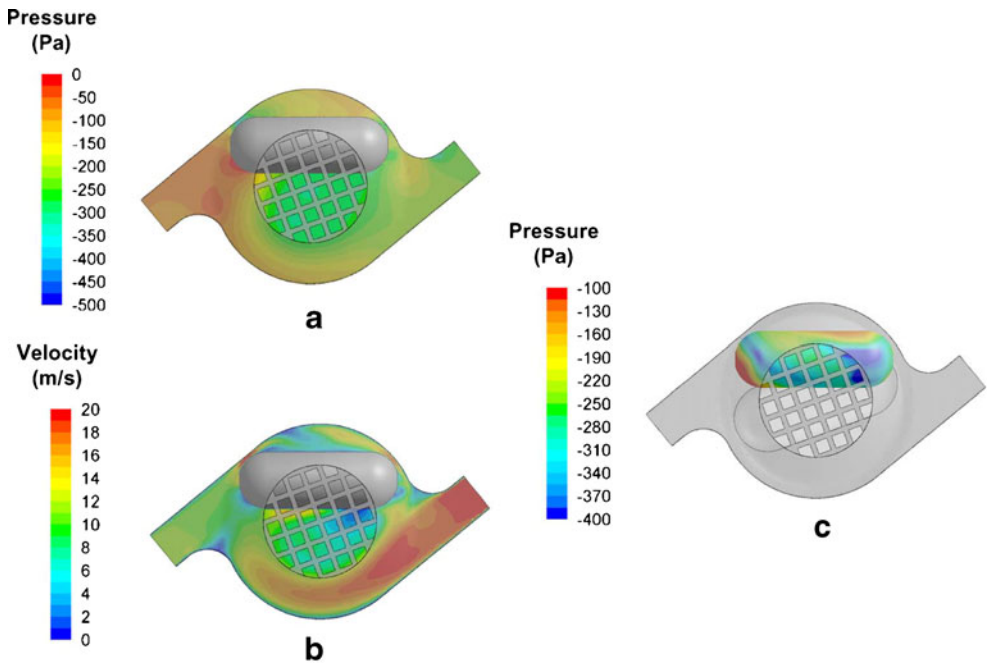

Fig. 3. CFD predictions of **a** the pressure and **b** velocity profiles within the Cyclohaler, as well as **c** the pressure profile of the whole capsule within the Cyclohaler at 39 l/min. The pierced holes in the capsule are not shown due to the orientation of the capsule

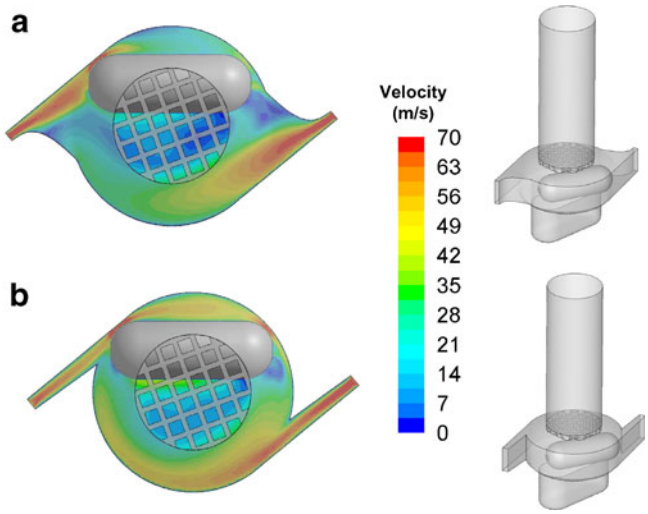

Fig. 4. Schematic illustrations and predictions of the velocity profiles within the **a** Mod 1 and **b** Mod 2 at 39 l/min

dimensions of the tangential inlets are expected to influence the specific resistance and flow field of the Cyclohaler.

The consequence of this cyclonic flow pattern in the capsule chamber results in the capsule experiencing a rotational force, as shown in the pressure differentials across the capsule (Fig. 3c). The greatest pressure difference occurred at the hemispherical regions of the capsule, suggesting the capsule moves across a rotational axis and experiences an axial force during rotation. This is consistent with the sequential high-speed video images of the capsule motion within the Cyclohaler, which shows that the capsule largely rotates tangentially around the capsule chamber with its long axis aligned with the tangential direction (Fig. 2 in Supplementary Materials).

The two design modifications (Mod 1 and Mod 2) were chosen as part of a systematic analysis of the design variables. The modifications made to Mod 1 and Mod 2 were produced by narrowing the air inlets, and Mod 2 was further modified by extending the narrow region of the air inlets (Fig. 4a and b). As a result of these modifications, the specific resistance of Mod 1 and 2 match that of HandiHaler (Fig. 5). The specific resistances of HandiHaler and Cyclohaler here agree reasonably well with the reported values in the literature (17,21). However, the CFD analysis shows noticeable differences between the flow behavior within the capsule chamber of Mod 1 and Mod 2. Specifically, the velocity profiles in Fig. 4a and b show higher air velocities near the inner wall of the capsule chamber in Mod 2 compared to Mod 1.

Cascade Impaction Testing

Table I and Fig. 6a–c show the ED, ISM, MMAD, GSD, and individual site deposition of tiotropium bromide monohydrate, aerosolized from commercial Spiriva capsules in the HandiHaler, Cyclohaler, Mod 1, and Mod 2 at 20, 39, and 55 l/min. For the Handihaler, the EDs±SD at 20, 39, and 55 l/min are 11.4±0.4, 13.0±0.5, and 11.9±0.2 μg, respectively. The ISMs± SD at 20, 39, and 55 l/min are 4.3±0.1, 5.2±0.4, and 5.3±0.2 μg, respectively. The mean MMAD decreases by approximately 30% (i.e., from 5.8 to 3.9 μm) as the flow rate increases from 20 to 55 l/min, indicating that more fine particles were generated at the higher flow rates. The aerodynamic particle size distribution (APSD) data demonstrate the flow rate dependence on the performance of the HandiHaler device.

The EDs of the drug from the Cyclohaler are about 14% and 15% less than that of HandiHaler at 20 and 39 l/min, respectively, although the differences in ISM of the two devices are less than 10% at these two flow rates. At all three flow rates, the drug depositions in the Cyclohaler device are at least two times greater than that in the HandiHaler device. Aerosolization of the drug from Spiriva capsules in the Cyclohaler at 55 l/min results in approximately 130% and 40% greater drug deposition on CI stages 1 and 2, respectively, and hence a much larger MMAD (i.e., 5.1 μm) in comparison to the HandiHaler.

The EDs±SD of the drug from Mod 1 at 20, 39, and 55 l/min are 9.4±0.1, 8.9±0.2, and 9.8±0.2 μg, respectively. At each of the three flow rates tested, the ED of Mod 1 is considerably lower than that of the HandiHaler. Differences in the ED of Mod 1 and HandiHaler range from about 17% to 32%. In contrast, the ISMs of Mod 1 are within approximately 12%, 4%, and 2% of those of the HandiHaler

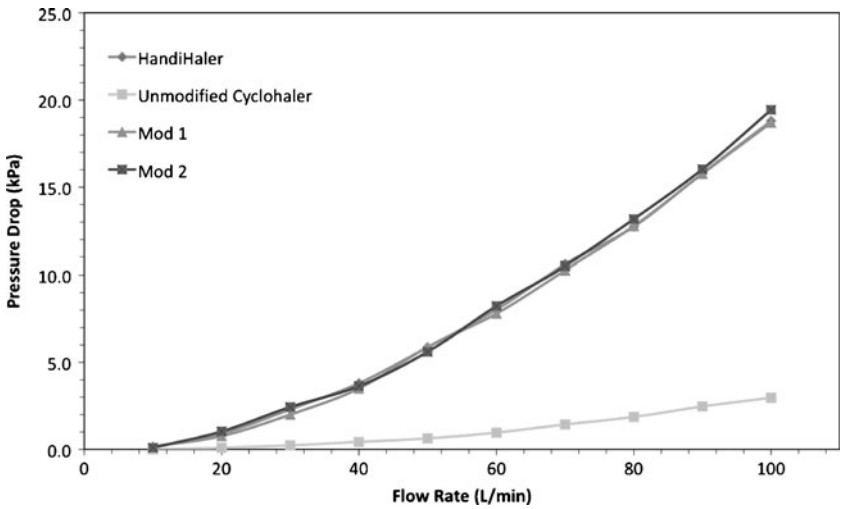

Fig. 5. The relationships between the pressure drop and flow rate for the HandiHaler, Cyclohaler, Mod 1, and Mod 2

Table I. ED, ISM, MMAD, and GSD of Tiotropium Bromide Monohydrate Following Aerosolization of Spiriva Capsules from the HandiHaler, Cyclohaler, Mod 1, and Mod 2 into the NGI at 20, 39, and 55 l/min ($n=3$)

	HandiHaler				Cyclohaler				Mod 1				Mod 2			
Flow rate (l/min)	ED, µg (max, min)	ISM, µg (max, min)	MMAD, µm (max, min)	GSD (max, min)	ED, µg (max, min)	ISM, µg (max, min)	MMAD, µm (max, min)	GSD (max, min)	ED, µg (max, min)	ISM, µg (max, min)	MMAD, µm (max, min)	GSD (max, min)	ED, µg (max, min)	ISM, µg (max, min)	MMAD, µm (max, min)	GSD (max, min)
20	11.4 (11.0, 11.8)	4.3 (4.1, 4.5)	5.8 (5.6, 5.9)	1.7 (1.7, 1.8)	9.8 (9.7, 10.0)	4.3 (3.9, 4.6)	5.7 (5.4, 6.1)	1.7 (1.7, 1.7)	9.4 (9.3, 9.5)	4.8 (4.7, 4.9)	4.7 (4.7, 4.7)	1.8 (1.7, 1.8)	12.5 (12.0, 12.9)	4.4 (4.3, 4.6)	5.8 (5.7, 5.9)	1.8 (1.8, 1.8)
39	13.0 (12.6, 13.5)	5.2 (4.7, 5.9)	4.1 (4.0, 4.3)	1.8 (1.8, 1.9)	11.1 (10.2, 12.1)	5.6 (5.3, 5.9)	4.2 (3.9, 4.5)	1.8 (1.7, 1.8)	8.9 (9.2, 9.4)	5.0 (5.0, 5.2)	3.9 (3.8, 4.0)	1.8 (1.8, 1.9)	13.6 (13.5, 13.7)	5.4 (5.1, 5.7)	4.1 (4.1, 4.2)	1.9 (1.9, 1.9)
55	11.9 (11.8, 12.0)	5.3 (5.2, 5.5)	3.9 (3.8, 4.0)	1.8 (1.8, 1.9)	10.9 (10.8, 11.0)	4.7 (4.6, 4.8)	5.1 (5.0, 5.1)	2.0 (2.0, 2.1)	9.8 (9.6, 9.9)	5.2 (5.1, 5.3)	3.5 (3.5, 3.6)	1.9 (1.9, 1.9)	11.8 (11.7, 12.0)	5.2 (5.1, 5.3)	3.7 (3.5, 3.8)	1.8 (1.8, 1.9)

ED emitted dose, *ISM* impactor-size mass, *MMAD* mass median aerodynamic diameter, *GSD* geometric standard deviation, *min* minimum, *max* maximum, *Mod 1* modification 1, *Mod 2* modification 2

at 20, 39, and 55 l/min, respectively. The Mod 1 MMAD is noticeably (i.e., approximately 19%) lower than that of the HandiHaler at 20 l/min. Individual site deposition data shown in Fig. 6a–c indicate appreciable differences in drug deposition in the mouthpiece adaptor and throat and/or pre-separator (i.e., about 17% to 64%) between Mod 1 and HandiHaler at the three flow rates.

In contrast to Mod 1, Table I and Fig. 6 show that the *in vitro* performance of Mod 2 is noticeably closer to HandiHaler. The ED, ISM, and MMAD of Mod 2 are within 10% of those of HandiHaler at all three flow rates. In addition, the mass deposited on each CI stage (i.e., stages 1–8) is very similar between Mod 2 and HandiHaler. Specifically, at all three flow rates, the differences in the mass deposited on stages 1, 2, 3, 4, and 5 of these two DPIs are less than 15%, except on stage 1 at 55 l/min (i.e., approximately 23% difference). Note that the sum of masses deposited on stages 1–5 constitutes at least 95% of the total mass deposited on stages 1–8. In addition to a high degree of similarity in the stage deposition, the drug depositions in the mouthpiece adaptor and throat, as well as the pre-separator, were also similar. In addition, drug deposition in the Mod 2 device is reduced and becomes closer to that of the HandiHaler (Fig. 6).

DISCUSSION

This study shows that the Cyclohaler and HandiHaler, which differ significantly in terms of the specific resistance, demonstrate noticeable differences in their aerosolization performance, provided that the same reference product formulation and capsule (Spiriva) was used for all cases. Specifically, the magnitudes of the differences within the CI between these two DPI devices appear to be flow rate dependent and become most pronounced in the drug deposition in the upper stages (stages 1–4) of the CI at 55 l/min (Fig. 6). The marked difference in these CI stages may be due to a greater aerosolization efficiency of the high-resistance HandiHaler at a higher flow rate. This enhanced efficiency is reflected in the CI data that show a lower MMAD for the HandiHaler (3.9 µm) in comparison to that for the Cyclohaler (5.1 µm) at 55 l/min. The above observations suggest that the specific resistance of the Cyclohaler may be one of the key factors that can affect the *in vitro* comparability of the test and reference DPI devices.

As indicated in the CFD analysis, the dimension and shape of the two air inlets of the Cyclohaler constitute key design parameters that control the pressure drop and airflow within the device. Therefore, as a step toward achieving *in vitro* comparability between the test and reference DPI devices, two modifications (Mod 1 and Mod 2) were made by manipulating the two air inlets of the Cyclohaler to match the specific resistance of the HandiHaler. These two modified Cyclohaler devices were also designed in an attempt to investigate the possible effect of different cyclonic flow conditions on the fluidization and deaggregation process within the device and their subsequent impact on their *in vitro* comparability to the HandiHaler. It is interesting to note that using the Spiriva capsule and formulation, Mod 1 and Mod 2 show considerable differences with regard to the degree of *in vitro* comparability to the HandiHaler, even though the specific resistance of these two test DPI devices is comparable to that of the reference DPI device. The CI data show that for the purpose of achieving

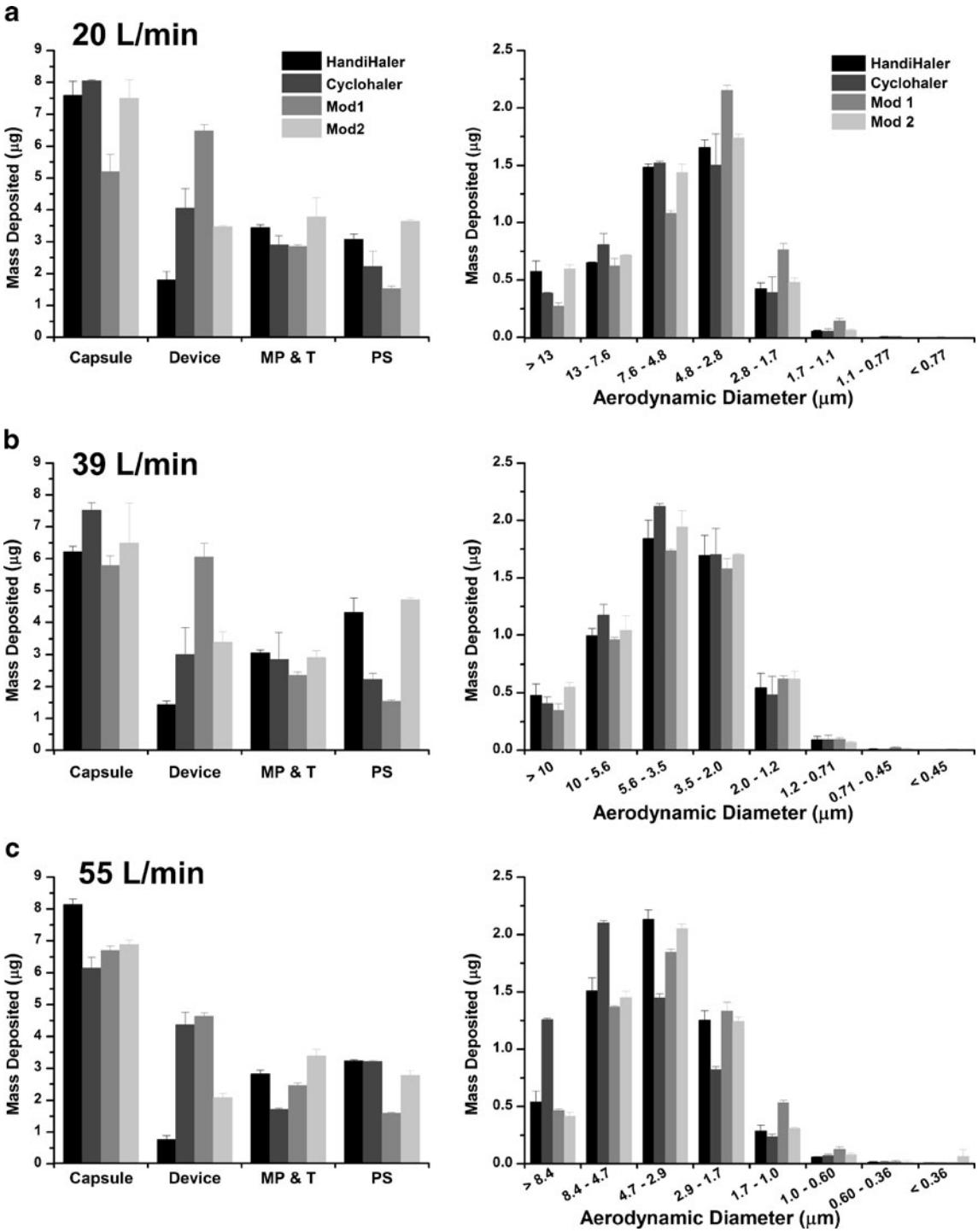

Fig. 6. Stage by stage deposition of tiotropium bromide monohydrate following aerosolization of Spiriva capsules from the HandiHaler, the Cyclohaler, Mod 1, and Mod 2 into the NGI at **a** 20, **b** 39, and **c** 55 l/min. *MP* and *T* represent mouthpiece and throat, while *PS* represents pre-separator. *Error bars* in graphical representations of data represent ±1 standard deviation (SD)

in vitro comparability to the HandiHaler, Mod 1 did not offer noticeable improvement over the Cyclohaler, while Mod 2 provided improved *in vitro* matching relative to the other test devices, especially at the flow rate of 55 l/min (Fig. 6c). This observation points out that from a device design perspective, matching the specific resistance of test and reference DPIs alone may not provide sufficient assurance for attaining comparable aerosolization performance.

In order to gain further understanding of underlying factors that determine the aerosolization performance of the HandiHaler, Cyclohaler, Mod 1, and Mod 2 and their *in vitro* comparability, carrier particle trajectories were simulated through these DPI devices to compare the fluidization and deaggregation process within the devices. Three variables, which may play a key role in determining the fluidization and deaggregation process in capsule-based DPI devices, were

Table II. CFD Predictions for the Capsule Force, Capsule Flow Rate, and Maximum Impact Velocity for the HandiHaler, Cyclohaler, Mod 1, and Mod 2

	HandiHaler			Cyclohaler			Mod 1			Mod 2		
Flow rate (l/min)	F_c (mN)	Q_c (l/min)	V_n (m/s)	F_c (mN)	Q_c (l/min)	V_n (m/s)	F_c (mN)	Q_c (l/min)	V_n (m/s)	F_c (mN)	Q_c (l/min)	V_n (m/s)
20	0.04	0.5	4.5	0.5	0.3	3.3	1.3	1.2	8.9	3.2	0.9	5.2
39	18.9	1.3	8.4	2.3	0.5	6.8	4.7	2.3	16.2	11.3	1.6	8.6
55	50.0	2.0	13.1	4.8	0.7	9.5	9.8	3.2	22.0	21.5	2.1	11.6

F_c capsule force, Q_c capsule flow rate, V_n maximum impact velocity

calculated based on the CFD airflow distributions and particle tracking data. They include (1) the flow rate of air through the pierced capsule (Q_c, l/min), which were determined as described in the "Materials and Methods" section; (2) the force exerted on the capsule (F_c, mN), calculated by integrating the pressure distribution over the total surface area of the capsule; and (3) the maximum particle impact velocity that represents the average of the maximum normal velocity component (i.e., perpendicular to the inhaler surface) of a carrier particle colliding into the inhaler surface (V_n, m/s).

The first two CFD performance measures are primarily related to the excitation of the powder within the pierced capsule and the entrainment of the powder from the pierced capsule. The third CFD performance measure is used to characterize the nature of the impacts during carrier particle–inhaler collisions, which were previously suggested to be one of the dominant factors in inducing deaggregation of drug particles from lactose carriers in DPI devices (15,30). These CFD performance measures, as summarized in Table II, are intended to illustrate important trends in the aerosolization performance of the DPI devices rather than to provide quantitative analysis. They provide some insights on the key aspects of the fluidization and deaggregation process in the HandiHaler, Cyclohaler, Mod 1, and Mod 2 (Table I) and their impact on *in vitro* comparability, as explained below.

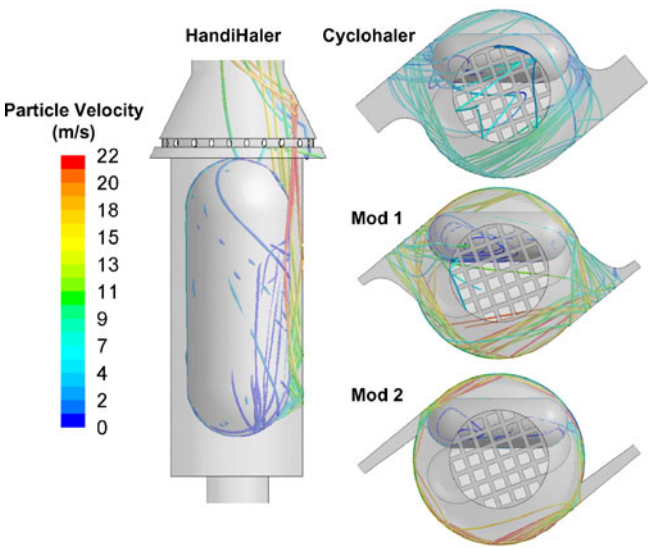

Fig. 7. Particle tracks of the 50-μm particles in the HandiHaler, Cyclohaler, Mod 1, and Mod 2 at 39 l/min

The influence of airflow rate on the capsule force is more pronounced in the HandiHaler device than it is in any of the three test devices. This may be related to the different modes of capsule vibration and movement in the test and reference DPI devices, which are predominantly rotational in the three test DPI devices (Cyclohaler, Mod 1, and Mod 2) and axial in the HandiHaler. However, there is no trend observed between this CFD performance measure and CI data, suggesting that it does not appear to play a significant role in determining the *in vitro* comparability of the three test DPI devices to the HandiHaler.

Although the specific resistances of Mod 1 and Mod 2 are comparable, differences in the capsule chamber geometries and the flow conditions between these two DPI devices result in noticeable differences in the flow rate of air through the pierced capsule and the carrier particle trajectories. Mod 1 and Mod 2 show appreciable differences in Q_c due to differences in the capsule chamber flow conditions. Table II shows that Q_c is 30% to 50% higher in Mod 1 than that in Mod 2. In addition, as illustrated in Fig. 7, the majority of carrier particles impact the inhaler surface in the Mod 1 device at relatively acute angles compared to the Mod 2 device, in which most carrier particle–inhaler collisions occur at relatively oblique angles. These oblique carrier particle–inhaler collisions observed in Mod 2 likely contribute to the reduced normal component of the impact velocity in the DPI device. This reduction in the normal impact velocity is reflected in the V_n data shown in Table II, which shows that V_n for Mod 2 is about 45% lower than that in Mod 1. As a result of these differences, Mod 2 shows the highest degree of similarity to the HandiHaler in terms of the Q_c and V_n for all three flow rates (Table II) among the three test DPI devices investigated in this study. These similarities correspond to the improved comparability of Mod 2 to the HandiHaler, as shown in the CI measurements.

Based on the CFD analysis and the APSD data, matching the resistance of devices is not sufficient to attain comparable *in vitro* performance. The current study highlights that an understanding of device aerosolization characteristics is also important with respect to establishing *in vitro* comparability for DPIs.

CONCLUSIONS

The present study shows that *in vitro* comparability can be achieved for two apparently different unit-dose, capsule-based test and reference DPI devices, Cyclohaler and HandiHaler, respectively, through appropriate modifications of the key attributes of the test DPI device (Mod 2) at the flow rates

of 20, 39, and 55 l/min. CFD modeling and *in vitro* characterization by a multistage cascade impactor were utilized to provide engineering assistance in identifying and understanding the key performance attributes, which would influence the criteria for designing and modifying a test DPI device. This investigation illustrates the importance of enhanced product understanding in the fabrication and refinement of a test DPI device that provides a closer match to the aerosolization performance of the reference DPI device at multiple flow rates.

ACKNOWLEDGMENTS

The authors would like to thank Bhawana Saluja for her valuable comments.

REFERENCES

1. Oversteegen L, Rovini H, Belsey MJ. Respiratory drug market dynamics. Nat Rev Drug Discov. 2007;6:695–6.
2. Daley-Yates PT, Parkins DA. Establishing bioequivalence for inhaled drugs; weighing the evidence. Expert Opin Drug Deliv. 2011;8:1297–308.
3. Lee SL, Adams WP, Li BV, Conner DP, Chowdhury BA, Yu LX. *In vitro* considerations to support bioequivalence of locally acting drugs in dry powder inhalers for lung diseases. AAPS J. 2009;11:414–23.
4. Chodosh S, Flanders JS, Kesten S, Serby CW, Hochrainer D, Witek Jr TJ. Effective delivery of particles with the HandiHaler dry powder inhalation system over a range of chronic obstructive pulmonary disease severity. J Aerosol Med. 2001;14:309–15.
5. Telko MJ, Hickey AJ. Dry powder inhaler formulation. Respir Care. 2005;50:1209–27.
6. Newman S, Busse WW. Evolution of dry powder inhaler design, formulation, and performance. Respir Med. 2002;96:293–304.
7. Byron PR, Hindle M, Lange CF, Longest PW, McRobbie D, Oldham MJ, *et al*. *In vivo–in vitro* correlations: predicting pulmonary drug deposition from pharmaceutical aerosols. J Aerosol Med Pulm Drug Deliv. 2010;23 Suppl 2:59–69.
8. Xu Z, Mansour HM, Mulder T, McLean R, Langridge J, Hickey AJ. Dry powder aerosols generated by standardized entrainment tubes from drug blends with lactose monohydrate: 2. Ipratropium bromide monohydrate and fluticasone propionate. J Pharm Sci. 2010;99:3415–29.
9. Clark AR, Hollingworth AM. The relationship between powder inhaler resistance and peak inspiratory conditions in healthy volunteers—implications for *in vitro* testing. J Aerosol Med. 1993;6:99–110.
10. Coates MS, Chan H-K, Fletcher DF, Raper JA. Effect of design on the performance of a dry powder inhaler using computational fluid dynamics. Part 2: Air inlet size. J Pharm Sci. 2006;95:1382–92.
11. Coates MS, Fletcher DF, Chan H-K, Raper JA. Effect of design on the performance of a dry powder inhaler using computational fluid dynamics. Part 1: grid structure and mouthpiece length. J Pharm Sci. 2004;93:2863–76.
12. Coates MS, Chan H-K, Fletcher DF, Raper JA. Influence of air flow on the performance of a dry powder inhaler using computational and experimental analyses. Pharm Res. 2005;22:1445–53.
13. Coates MS, Fletcher DF, Chan H-K, Raper JA. The role of capsule on the performance of a dry powder inhaler using computational and experimental analyses. Pharm Res. 2005;22:923–32.
14. Inthavong K, Choi L-T, Tu J, Ding S, Thien F. Micron particle deposition in a tracheobronchial airway model under different breathing conditions. Med Eng Phys. 2010;32:1198–212.
15. Wong W, Fletcher DF, Traini D, Chan H-K, Crapper J, Young PM. Particle aerosolisation and break-up in dry powder inhalers 1: evaluation and modelling of venturi effects for agglomerated systems. Pharm Res. 2010;27:1367–76.
16. Wong W, Fletcher DF, Traini D, Chan H-K, Crapper J, Young PM. Particle aerosolisation and break-up in dry powder inhalers: evaluation and modelling of impaction effects for agglomerated systems. J Pharm Sci. 2011;100:2744–54.
17. Donovan MJ, Kim SH, Raman V, Smyth HD. Dry powder inhaler device influence on carrier particle performance. J Pharm Sci. 2012;101:1097–107.
18. Longest PW, Holbrook LT. In silico models of aerosol delivery to the respiratory tract—development and applications. Adv Drug Deliv Rev. 2012;64:296–311.
19. Longest PW, Hindle M. Condensational growth of combination drug-excipient submicrometer particles for targeted high efficiency pulmonary delivery: comparison of CFD predictions with experimental results. Pharm Res. 2012;29:707–21.
20. Longest PW, Tian G, Walenga RL, Hindle M. Comparing MDI and DPI aerosol deposition using *in vitro* experiments and a new stochastic individual path (SIP) model of the conducting airways. Pharm Res. 2012 (in press).
21. Criée CP, Meyer T, Petro W, Sommerer K, Zeising P. *In vitro* comparison of two delivery devices for administering formoterol: Foradil P and formoterol ratiopharm single-dose capsule inhaler. J Aerosol Sci. 2006;19:466–72.
22. Shih T-H, Liou WW, Shabbir A, Yang Z, Zhu J. A new kappa-epsilon eddy viscosity model for high Reynolds-number turbulent flows. Comput Fluids. 1995;24:227–38.
23. Launder BE, Rodi W. The turbulent wall jet measurements and modeling. Annu Rev Fluid Mech. 1983;15:429–59.
24. ANSYS. ANSYS Fluent 6.3 Users Guide. Lebanon, NH, USA. 2006. At: http://hpce.iitm.ac.in/website/Manuals/Fluent_6.3/Fluent.Inc/fluent6.3/help/index.htm. Accessed 4 Nov 2010.
25. Zhang Y, Finlay WH, Matida EA. Particle deposition measurements and numerical simulation in a highly idealized mouth-throat. J Aerosol Sci. 2004;35:789–803.
26. Liu Y, Matida EA, Gu J, Johnson MR. Numerical simulation of aerosol deposition in a 3-D human nasal cavity using RANS, RANS/EIM, and LES. J Aerosol Sci. 2007;38:683–700.
27. Morsi SA, Alexander AJ. An investigation of particle trajectories in two-phase flow systems. J Fluid Mech. 1972;55:193–208.
28. US Pharmacopeia. <601> Aerosols. Metered-dose inhalers and dry powder inhalers: particle size. Rockville: US Pharmacopeia 35/National Formulary 30, United States Pharmacopeial Convention; 2012.
29. Wachtel H, Ertunc O, Koksoy C, Delgado A. Aerodynamic optimization of Handihaler and Respimat: the roles of computational fluid dynamics and flow visualization. In: Dalby R, Byron P, Peart J, Suman J, Farr S, Young P, editors. Respiratory drug delivery 2008. Illinois: Davis Healthcare International Publishing; 2008. p. 165–74.
30. Nichols S, Wynn E. New approaches to optimizing dispersion in dry powder inhalers-dispersion force mapping and adhesion measurements. In: Dalby R, Byron P, Peart J, Suman J, Farr S, editors. Respiratory drug delivery 2008. Illinois: Davis Healthcare International Publishing; 2008. p. 175–84.